Uludağ University Journal of The Faculty of Engineering, Vol. 23, No. 1, 2018 RESEARCH

DOI: 10.17482/uumfd.377444

PARAMETRIC INVESTIGATION OF HARNESSED POWER OF TWO TANDEM CYLINDERS IN FLOW INDUCED VIBRATION

Erinç DOBRUCALI [*]

Received: 11.01.2018; revised: 03.04.2018; accepted: 05.04.2018

Abstract: In transverse flow, cylinders respond in FIV (Flow Induced Vibrations); particularly VIV (Vortex Induced Vibrations) and galloping. Typically, in the galloping region, the hydrokinetic power converted to mechanical in the oscillators increases with increasing flow velocity and Reynolds number. Flow Induced Vibrations (FIVs) of two tandem, rigid and circular cylinder with end-springs are studied for 30,000<Re <120,000 with different damping, mass ratio and stiffness as parameters in the Low Turbulence Free Surface Water (LTFSW) Channel of the Marine Renewable Energy Laboratory (MRELab). Typical local drops and jumps in harnessed power were observed in the velocity range of 0.9<U<1.2 m/s within the galloping region. The main objective of this paper is to explain the reason for the presence of these drops and jumps. To achieve this objective, the points of changing in harnessed power in an extensive set of data with spacing, damping, stiffness, and flow velocity as parameters are identified. For both up and downstream cylinders, the harnessed power, amplitude-ratio, frequency-ratio and time history graphs are obtained to define the reason of these drop/jumps. Visualization with high-resolution camera has been used and the assumption which may affect the phenomena were studied and presented. Galloping instability disappears at this drops and harnessed power decreases sharply and amplitude as well. As a conclusion, there is a big interaction between cylinders.

Keywords: Vortex Induced Vibrations, galloping instability, harnessed power.

Akış kaynaklı titreşimde iki ardışık silindirden elde edilen gücün parametrik olarak incelenmesi

Öz: Enine akışlarda silindirler özellikle çevri kaynaklı titreşim ve hızlı artış (galloping) adı verilen bölgeden oluşan akış kaynaklı titreşim sergilerler. Hızlı artış bölgesinde, osilatörlerde mekanik enerjiye çevrilen hidrokinetik enerji akışın hızı ve Re sayısıyla artar. Türbülanslı serbest su yüzeyli kanalda yapılan deneylerde arkalı önlü bulunan ardışık silindirlerin hareketi 30,000<Re <120,000 aralığında farklı parametreler için incelenmiş ve özellikle hızlı artış bölgesindeki 0.9<U<1.2 m/s akış hızı aralığında elde edilen güçte lokal artış ve düşüşler tespit edilmiştir. Bu çalışmanın amacı bu artış/azalışların sebeplerini açıklamaktır. Bunun için tüm deneyler incelenerek bu ani değişim olan parametreler (Kütle oranı, yay sabiti, hız oranı vb. gibi) belirlenerek bir matris oluşturulmuştur. Hem öndeki silindir hem de arkasındaki silindir için elde edilen güç, genlik oranı, frekans oranları ve zamana bağlı hareket grafikleri oluşturulmuştur. Yüksek çözünürlüklü kamera ile görüntüleme tekniği kullanılmış ve elde edilen sonuçlar tartışılmıştır. Bu değişimlerin ana sebebinin iki silindir arasındaki etkileşim olduğu tespit edilmiştir. Bu değişimlerde hızlı artış dengesizliği kaybolmakta ve elde edilen güçte ve genlikte ani düşüşler oluşmaktadır.

Anahtar Kelimeler: Çevri kaynaklı titreşim, hızlı artış dengesizliği, güç.

[*] Istanbul Naval Shıpyard, Pendik, 34890, Istanbul, TURKEY. Correspondence Author: Erinç DOBRUCALI (edobrucali@yahoo.com)

1. INTRODUCTION

Flow Induced Vibrations (FIVs) present a source of challenge for various structures in steady flows such as bridges, buildings, heat exchangers, offshore structures, or power transmission cables. Unlike previous efforts to control the occurrence of Flow Induced Vibrations (FIV), which is a potential harmful phenomenon for structures subjected in a flow, VIVACE utilizes and enhances FIV to harnessed power from river and ocean currents. VIV and galloping are the most well-known phenomenon of FIV with different features. Vortex-induced vibration (VIV) occurs when shedding vortices (e.g. the Von Karman vortex street) creates pressure differences and couples with the restoring force (e.g. spring stiffness) on a cylinder in cross-flow to both flow and structure. It can occur over a large range of Reynolds numbers (Re). Galloping is an aero/hydro-elastic instability, which is described by high amplitudes and lower frequencies than VIV and is perpendicular to the flow. It is more robust and destructive than VIV. Galloping does not depend on vortex formation, occurs above a critical flow velocity, and has a bigger amplitude of oscillation. Elastic bodies with circular cross section in a flow usually experience VIV, while galloping occurs on a body with non-circular cross section (Blevins, 1990). Depending on the flow speed, the geometry of the body and the oscillator parameters, these two FIVs may coexist in a transition part between them, may overlap, or may be separated (Bernitsas at al., 2007, Chang, 2011, Kinaci et al, 2016, Park et al, 2013a-b).

As mentioned, in many engineering applications, FIVs are suppressed because of their destructive nature. MRElab managed to convert the kinetic energy of water flows into electricity by enhancing FIV (Bernitsas at al., 2007, Chang, 2011, Bernitsas and Raghavan 2009,2011, 2014, Raghavan 2007). In MRElab, Flow Induced Vibrations (FIV) is studied to convert marine hydrokinetic energy, from oceans, tidal and rivers to electricity using the VIVACE energy harvester. Vortex Induced Vibrations for Aquatic Clean Energy Converter is probably the closest to commercialization because it has suffered extensive laboratory testing and much field deployments since its introduction in 2006. The objective of the Marine Renewable Energy Lab (MRELab) is to investigate FIV of single and multiple cylinders and find different ways to enhance FIV in order to design VIVACE Converters and optimize the power output for various flow velocities.

Vortex-induced vibration (VIV) to a cylinder has been studied experimentally (Park et al. (2013a-b), Park et al. (2012), Kim et al. (2013), Park et al. (2012)) and numerically (Wu (2011), Wu (2011), Ding et al. (2013, 2015)) by researchers in order to eliminate or at least regulate this unsteady fluid-structure interaction phenomenon since it has been identified as the cause for many structural failures. But, it is challenging, and it is still being debated due to the complexity of the interaction between body dynamics and fluid dynamics. Two cylinders arrangement have been studied in many types of research as the simplest arrangement. In this research, both cylinders can oscillate which has not been done very often in previous papers up to now. Moreover, most of the previous experiments on VIV were conducted in TrSL2 regime which fluctuating lift coefficient rises as the Re increases. But in this research, experiments placed in TrSL3 that shear layer becomes fully turbulent, and the fluctuating lift coefficient of a smooth cylinder reaches its maximum value.

There are many fundamental differences in the flow dynamics past a cylinder between the TrSL3 and TrSL2 flow regimes as defined by Zdravkovich (1997, 2002). The shear layers on both side of the cylinder are saturated in TrSL3 transporting more vorticity to the Von Kármán vortices. Thus, the shear layers have a stronger roll-up much closer to the cylinder. The circulation in the von Kármán vortices arives shedding strength faster since the Strouhal number (Nrel (2012)) is about constant over the whole laminar flow regime for $400<Re<300,000$. Thus, the vortex shedding frequency rises proportionally to the flow velocity. Further, the formation length is shorter. (Unal and Rockwell, 2012) The combination of a shorter formation length with a strong roll-up and higher circulation closer to the after the cylinder body cross-section

induces higher lift force at the moment of shedding. Thus, as shown in Figure 1a and b. below, the lift coefficient in TrSL3 is many times higher than that in the TrSL2 part.

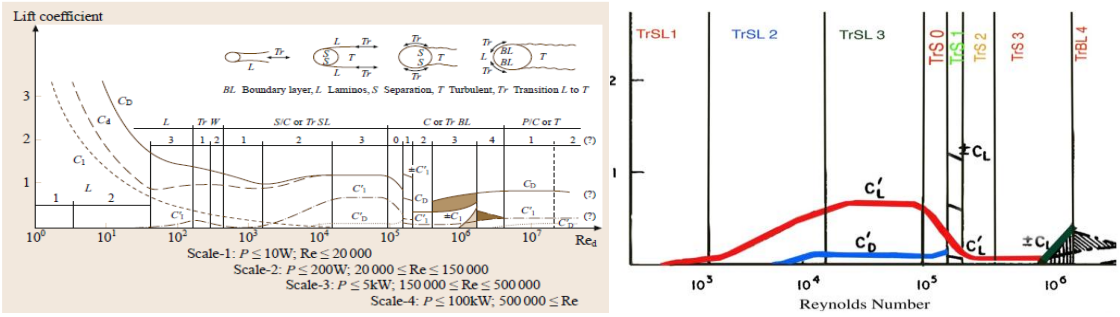

a. *b.*

Figure 1. a) Variation of force coefficients for disturbance-free flow ***b)*** Mean lift (C_L) coefficient, fluctuating lift (C'_L) and drag (C'_D) coefficients and in the TrSL and TrBL regimes (Reproduced from (Zdravkovich (1997), Bernitsas (2016))

Bokaian and Geoola (1984) considered the case of fixed upstream cylinder and flexible downstream cylinder. They presented that "depending on the cylinders separation", and structural damping, the downstream cylinder exhibited 1) a vortex-resonance, 2) a galloping, or a combined vortex-resonance and galloping, or 3) a separated vortex-resonance and galloping" response. They found high amplitude responses which they stated "wake-induced galloping". They also demonstrated that whilst some characteristics of wake-excited galloping were defined to be the same to those of galloping of sharp-edge cylinder bodies, the others were observed to be basicly different.

Sun et al. (2015) investigated the fluid-structure coupling between two circular cylinders in tandem at a different spacing from L/D = 1.2-6.0. Based on the galloping vibrations generated, four regimes are identified. Regime I (L/D ≤ 1.5) is defined by both cylinders experiencing the downstream cylinder vibration amplitude and galloping vibrations smaller than the upstream one. At regime II (1.5 < L/D < 2.5), the galloping vibration is larger for the upstream cylinder than the downstream one at smaller Ur, but the opposite dominates at larger Ur. At regime III (2.5 ≤ L/D ≤ 3.0), the downstream cylinder vibration amplitude is larger than the upstream one and the upstream cylinder shear layer reattachment takes place on the front surface of the downstream one. Regime IV (L/D > 3.0) features small vibration for the downstream cylinder induced by convective vortices from the upstream cylinder and no vibration for the upstream cylinder.

In this paper, variation in harnessed power in the velocity range of 0.9 < U < 1.2 m/s for two tandem cylinders with PTC (Passive Turbulence Control) were investigated. To achieve this goal, the data of mechanical energy which converted from hydrokinetic to mechanical as a function of reduced velocity, Re and the flow speed were used. (Sun et al., 2017) The simulated Re range for which experiments were done in the MRELab is 30,000< Re < 120,000, which places in the TrSL3 regime. Critical points, which dramatically drop or jump in power conversion were chosen and visualized by a high-resolution camera. Harnessed power, amplitude ratio, frequency ratio and time histories at point of drops and jumps were evaluated and presented. All the vortices which shed from sides of the upstream cylinder toward downstream cylinder were observed by regarding captured videos frame by frame. The experimental set-up is described in Section 2 including the facility, the oscillator, Vck and the Passive Turbulence Control (PTC). A mathematical model is represented in Section 3, results and discussions are explained in Section 4.

2. EXPERIMENTAL DETAILS

In this section, The Low-Turbulence Free Surface Water (LTFSW) channel, cylinders used in this experiment, virtual damper-spring (V_{ck}) system, flow visualization set-up, data collection and experimental matrix are presented briefly.

2.1. LTFSW Channel

LTFSW channel of the Marine Renewable Energy Laboratory (MRElab) at the University of Michigan was choosed for the model tests of the VIVACE Converter. The channel has the potential to re-circulates about 37,854 liters of water at speed up to 1.4 m/s by an impeller powered by a 20hp induction motor. The test section is 2.44 m long, 1 m wide and 1.52 m deep and made of transparent flex-glass, thus, allowing for visualization of the VIV and galloping characteristics. The stoppers were installed to keep safe the bottom flex-glass of the test section from breaking by the cylinder impact. A schematic of the LTFSW Channel is shown in Figure. 2.

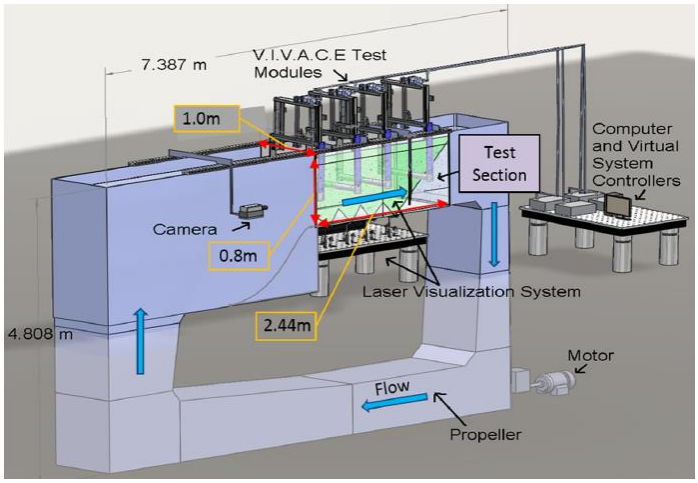

Figure 2. Schematic of the LTFSW channel.(Kim and Bernitsas 2016)

2.2. Cylinders and PTC

Two PTC circular cylinders of diameter D = 0.0889m and length L = 0.914m was utilized for this experiments. An evaluation of blockage effects was studied by Kinaci et al. (2016) shown in Figure. 3, the test cylinders were mounted on two linear end springs and the cylinder motion was allowed in the cross-flow direction only. In this study, center to center distance between two cylinders is between 1.57D and 2.57D. Specific design of the two single-cylinder Converter modules is listed in Table 1. The added mass inclusion through a constant added mass coefficient (from potential theory) is still debated (Vikestad et., 2000). In this study, it is accepted that added mass coefficient as equal to 1. It also has a power take-off (PTO) system consisting of a heat bank for dissipation of the generated energy. The excitation comes from the fluid-structure interaction (FSI) and is applied to the cylinders throughout the forces imparted by the motion of the fluid.

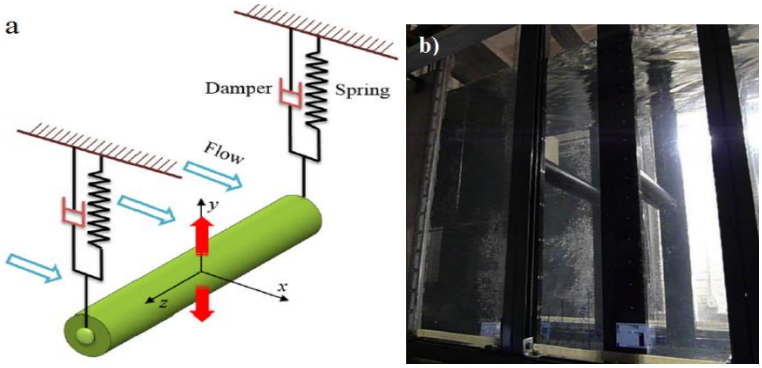

Figure 3. VIVACE Converter in the LTFSW Channel with V_{CK} system: **a)** Schematic of a single-cylinder VIVACE Converter and **b)** Two-cylinders (Bernitsas, 2016)

Table 1. Particulars of two cylinders VIVACE Converter

Parameters	**Symbol**	**1st device**	**2nd device**
Diameter	D(m)	0.0889	0.0889
Length	L(m)	0.914	0.914
Oscillating mass	m(kg)	7.286	7.286
Spring Const.	k(N/m)	400-1,200	400-1,200
Sys. Damping ratio	ζ	0.06-0.26	0.06-0.26
Total Damping	C_{total}(Ns/m)	8.55	64.22
Natural Freq. in water	$F_{n,w}$	0.97~ 1.67	0.97~ 1.67
Displaced Fluid mass	m_d(kg)	5.425	5.425
Mass ratio	m^*	1.343	1.343
Added Mass	m_a(kg)	5.425	5.425
Added Mass coefficient	C_a	1	1

To enhance the FIV of the cylinder, distributed roughness in the form of roughness bands was introduced and investigated in the MRELab experimentally (Bernitsas and Raghavan 2011, Park 2012) and numerically (Zdravkovich 1997, 2002). Passive Turbulence Control (PTC) was distributed surface roughness in the form of two straight roughness bands and study resulted in a valuable tool, the PTC-to-FIV Map (Park, 2012). The roughness strips used in this paper were commercially available and designated as P60 as shown in Figure 4. The details of PTC are explained in the study of Chang (2010). Also, it should be noted the results of previous studies (Park et al., 2012, 2013a, 2013b) on PTC, bands with commercial roughness designation P60 and width of 12.7 mm, which covers 16^0 on both side of the 88.9 mm diameter cylinder were used in this study. The total thickness of the PTC is on the order of the boundary layer thickness. PTC has an impact on the energy conversion and the efficiency of the VIVACE.

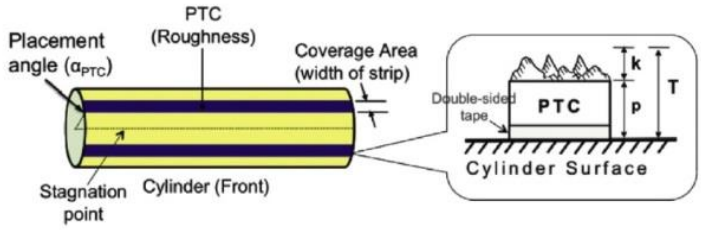

Figure 4. Configuration of the PTC on the cylinder (Chang, 2010).

2.3. Virtual Damper-Spring (V_{ck}) System

In previous investigations on a single-cylinder VIVACE Converter, the power was measured by introducing additional harness damping into the Converter using the virtual damper-spring (V_{ck}) system (Lee and Bernitsas 2011, Chang, 2010, Lee et al., 2011). The V_{ck} system changed the real springsand the real damper of the Converter system. More details of the V_{ck} system can be obtained in the paper by Lee et al., (2011) and Sun et al., (2015). MRELab has conducted tests with a single cylinder Converter by changing damping ratio and the spring stiffness K by using the V_{ck} system over the entire range of flow velocity. The oscillating mass m_{osc} of the oscillator encompasses the cylinder mass, one third of the equivalent mass of transmission belts and pulleys. For all experiments, the V_{ck} system utilized in systematic testing for generation of harnessed power envelopes of the two-cylinder converter instead of physical linear springs.

2.4. Data collection

The oscillation frequency f_{osc} is calculated by Fast Fourier transform (FFT) of the displacement of the cylinder over the setted period with the lockout of the end-transients. The sampling rate of the data acquisition system is 1,000 Hz. For each speed of the flow, after steady state has been reached, 60 s of the displacement data are calculated. The amplitude and the corresponding standard deviation are calculated using the RMS of the 60 largest (negative and positive) amplitude measure. The f_{osc} is calculated by a Fast Fourier. For analyzing data, a camera (Sony-Rx 10 II) used to record approximately one-minute videos of each run. Two 5 W argon lasers and aluminum oxide particles of 100 mm used to understand the visualization better. Then the videos were break to frames to post-processing the complex phenomena as well as possible.

2.5. Flow Visualization set-up and Laser Arrangement

Qualitative tests are performed in the form of flow visualization besides quantitative measurements. The near-wake of the oscillating circular cylinder is studied to see the flow patterns and how they are related to the cylinder reaction under different conditions. Visualization of flow is done by mixing the suitlable amount of aluminum oxide particles of 100 μm in the LTFSW channel. Powder particles are mixed with fresh water in a container of appropriate size made for this purpose.

Laser arrangement for flow visualization in LTFSW can be seen in Figure 5. The laser beam emitted from an Argon Laser Unit is passed through a lens system and reflectors to obtain a homogeneously distributed laser light sheet to illuminate the test-section. Some adjustments are done in the laser power to optimize the light intensity depending on the flow velocity (Bernitsas, 2016).

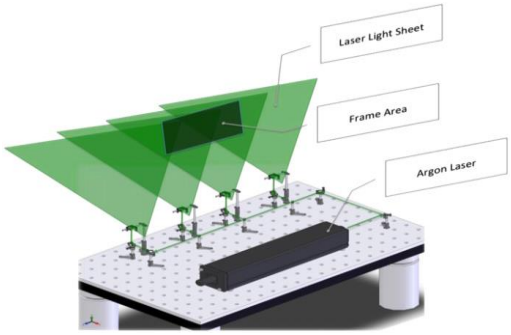

Figure 5. Laser Arrangement for flow visualization in LTFSW channel (Bernitsas, 2016) .

3. MATHEMATICAL MODEL

3.1 The Motion of the Cylinder

A mathematical model are presented in this section (Bernitsas, 2016, Bernitsas et al., 2008). Whereas the flow direction is the positive x-direction, the movement of the cylinder in the y-direction is modeled by a second-order linear differential equation as

$$m_{osc}\ddot{y} + c_{total}\dot{y} + ky = F_{fluid} \tag{1}$$

The m_{osc} is the total oscillating system mass, which includes one third of the spring mass, where y is the perpendicular direction to the flow and the cylinder axis, C_{total} is the total damping coefficient ,K is the spring stiffness and F_{fluid} is the force exerted by the fluid on the body in the y direction. To convert hydrokinetic energy to mechanical energy and subsequently electrical energy, additional damping is used in the system. The total damping (C_{total}) is defined as

$$C_{total} = C_{structure} + C_{harness} \tag{2}$$

Where $C_{stucture}$ is the existing damping due to losses in the transmission system, in this research, all the $C_{stucture}$ are adjusted by V_{ck} system according to m^* and K to achieve same artificial $\zeta_{structure}$, $C_{stucture}$ is the damping added through V_{ck} that converts the mechanical energy in the oscillating cylinder to electrical energy simulating the real flow.

From equation (2), $C_{stucture}$ and $C_{harness}$ can be expressed using damping ratio $\zeta_{harness}$ and $\zeta_{structure}$.

$$\zeta_{structure} = \frac{C_{structure}}{2\sqrt{m_{osc}K}} \tag{3}$$

$$\zeta_{harness} = \frac{C_{harness}}{2\sqrt{m_{osc}K}} \tag{4}$$

3.2 Fluid Power Conversion

Then mechanical power of VIVACE can be expressed as:

$$P_{VIVACE-Mech} = \frac{1}{T_{osc}} \int_0^{T_{osc}} 4\pi (m_{osc} + m_a) \zeta_{total} \dot{y}^2 f_{n,water} \, \mathrm{dt} \tag{5}$$

$$P_{VIVACE-structure} = 8\pi^3 (m_{osc} + m_a) \zeta_{structure} (A f_{osc})^2 f_{n,water} \tag{6}$$

Using equation (6), we obtain the harnessed power and the dissipated power as

$$P_{VIVACE-structure} = 8\pi^3 (m_{osc} + m_a) \zeta_{structure} (A f_{osc})^2 f_{n,water} \tag{7}$$

$$P_{VIVACE-dissipated} = \frac{1}{2} C_{structure} A^2 \omega_{odc}^2 \tag{8}$$

Since equations (7) and (8) appear to depend explicitly on the added mass ma, it is worth noting that they can be recast using as follows, respectively.

$$P_{VIVACE-dissipated} = \frac{1}{2} C_{structure} A^2 \omega_{osc}^2 \tag{9}$$

and

$$P_{VIVACE-harness} = \frac{1}{2} C_{harness} A^2 \omega_{osc}^2 \tag{10}$$

Where, A is the amplitude of the cylinder, ω_{osc} is the angular frequency, which can be measure using V_{ck} system.

4. RESULTS and DISCUSSION

In order to find the reasons for changes in harnessed power in galloping region, many experiments were done to calculate the flow induced vibrations of two cylinders in tandem with different parameters like spring stiffness, damping ratio, center-to-center spacing ratio (*L/D*) and the mass ratio ($m^* = 1.343$). The experimental parameters can be shown in Table 1. Absolute flow velocity (*U*) was between 0.35 m/s and 1.35 m/s. Re range was $30{,}000 \leq Re \leq 120{,}000$ which locates in the high-lift TrSL3 regime. But while evaluating the power harnessed results, typical local drops and jumps in harnessed power were observed in the velocity range of $0.9 < U < 1.2$ m/s within the galloping region. Table 2 shows the test matrix which exists these local drops and jumps for different *K*, damping ratios and spacing. Red, green and yellow boxes represent drops, jumps and no drop & jump, respectively. The numbers inside the boxes show the absolute velocity values which occur drop or jump.

In this study, some results are selected and evaluated further to find out the reason for these drops and jumps. To achieve this objective, the points of fluctuation in power harnessing in an extensive set of data with spacing, damping, stiffness, and flow velocity as parameters are identified and the harnessed power, frequency-ratio and amplitude-ratio results for both the up and downstream cylinders are used to locate the power drop/jump points and visualization with high-resolution camera have been used and the assumption which may affect the phenomena were studied and presented.

As mentioned, the main goal of this study is to find out the relationship between drops or jumps in absolute velocity range of especially $0.9 < U < 1.2$ m/s and L/D = 1.57, 2.01 and 2.57, which happens in the galloping region. As it was explained in previous part, three sets of experiments with three different spacing and their optimum K have been chosen. Figures 6 a-b-c show harnessed power as a function of the flow velocity. To facilitate understanding the results, the absolute velocity and reduced velocity which are proportional to Re, are also shown parallel

to the x-axis. In figures 6- a, b and c the black line indicates harnessed power for a single cylinder. A red line, blue line and green line present harnessed power for the upstream cylinder, downstream cylinder and synergy, respectively.

Table 2. Test Matrix existing local drops and jumps according to spacing (*L/D*) parameters.

L/D:1.57						
K	ζ = 0.04	ζ = 0.08	ζ = 0.12	ζ = 0.16	ζ = 0.20	ζ = 0.24
400	1.19	both	1.03	1.03	1.03	1.07
600	1.00	1.00	1.07	1.00	1.00	1.07
800	1.12	1.20	1.20	1.20	1.19	1.20
1,000	1.20	1.20	1.24	1.24	1.24	1.24
1,200	no drop	no drop	no drop	no drop	no drop	no drop
L/D:2.01						
400	no drop	both	1.20	1.15	1.20	1.16
600	1.15	1.16	1.16	1.16	1.12	1.12
800	no drop	no drop	1.16	1.15	1.15	1.16
1,000	no drop	1.15	1.15	1.15	1.23	1.16
1,200	1.06	1.06	1.06	1.06	1.06	1.06
L/D:2.57						
400	no drop	1.15	1.15	1.15	1.15	1.15
600	no drop	no drop	1.15	1.15	1.15	no drop
800	no drop	1.00	1.00	1.00	1.15	1.15
1,000	1.04	1.04	1.00	1.04	1.04	0.97
1,200	1.16	1.16	1.15	1.15	1.16	1.15

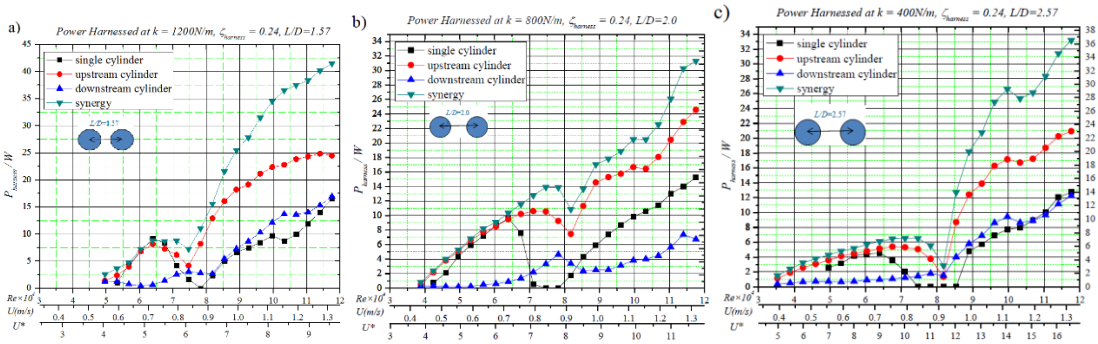

Figure 6. *Harnessed Power curves for m* = 1.343 and $\zeta_{harness}$ = 0.24* ***a)*** *with K = 1,200 N/m spacing L/D = 1.57* ***b)*** *with K = 800 N/m spacing L/D = 2.01* ***c)*** *with K = 400 N/m spacing L/D = 2.57 (Bernitsas, 2016b)*

As it shows in Figure 6 for L/D = 1.57 with K = 1,200, which is the optimal *K* and $\zeta_{harness}$ = 0.24, there are no drops in power graph for mentioned range. With increasing in *L/D* the drops and jumps, immediately after, will show up. So, the hypothesis will be that with increasing distance between two tandem cylinders, fluctuations will appear in the region of galloping and become stronger even more with increasing in distance. It means that for small pitch ratios (approx. 1 < *L/D* < 1.2–1.8 (Zdravkovich, 1987) or 1 < *L/D* < 2 (Zhou and Yiu, 2006), depending on the *Re* range) the two cylinders behave as a single body or ‘‘extended-body’’. It can be cliamed that close spacing yields the highest harnessed power and converted power because of the behaviour of two cylinders as a single body. The downstream sits inside the vortex formation region of the upstream cylinder (Zhou and Yiu, 2006) and the separated shear layers from the upstream one are forced to enclose or wrap around the downstream one, without any reattachment onto its surface, before rolling up alternately into Kármán vortices behind the downstream cylinder. For intermediate pitch ratios (approx. 1.2–1.8 < *L/D* < 3.4–3.8 (Zdravkovich, 1987) or 2 < *L/D* < 5 (Zhou and Yiu, 2006), depending on the range of *Re*, the cylinders are placed sufficiently far apart that the shear layers from the upstream cylinder can no longer enclose the downstream cylinder, but instead reattach onto the downstream cylinder. The downstream sits inside the vortex formation region of the upstream cylinder (Ishigai et al., 1972) and the separated shear layers from the upstream cylinder are forced to enclose or wrap around the downstream cylinder, without any reattachment onto its surface, before rolling up alternately into Kármán vortices behind the downstream cylinder. Figure 7 shows the classification of the flow pattern for two tandem circular cylinders in cross-flow, which presents study placed in “extended-body” and “reattachment” regime as mentioned.

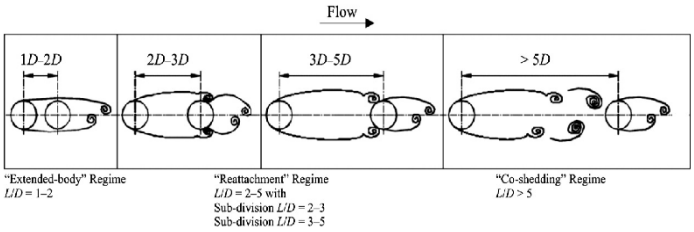

Figure 7. *Simplified classification scheme of the flow patterns for two tandem circular cylinders in cross-flow, from (Xu and Zhou, 2004) and (Zhou and Yiu, 2006).*

For further investigation, a camera (Sony-Rx 10 II) used to record 1-minute videos of each experiment. The path and direction of each particle was determined. Then, the videos were broken into frames in order to post-processing the complex phenomena as well as possible. It should be mentioned; in this case, both cylinders experience galloping vibrations and the oscillation of both cylinders is in phase.

Absolute velocity *U* = 1.121 m/s was selected from graphs in Figure 7 and investigated by visualization in all three spacing. Process of each experiment is explained below. In Figure 8, the flow pattern around two tandem cylinders is schematically drawn.

In most cases, the pattern for *L/D* = 1.57 would be similar to Figure 8-a. There is no gap flow between two tandem cylinders and both cylinders act like a single body. In Figure 8-b and c the flow pattern are shown for *L/D* = 2.01 and 2.57, respectively. In this case, for the interaction of two cylinders, the shear layer from one cylinder directly interacts the other cylinder surface by reattaching. Depends on the space between two cylinders; the downstream cylinder is partially or completely submerged in the wake of the upstream one. In most situations, upstream cylinder sheds in the space between two cylinders, forming alternate vortices. In this case, the alternate vortices from the upstream cylinder do not hit the downstream cylinder during passing on the cylinder. The interaction is generally very powerful, and it intensifies fluctuating drag and lift significantly.

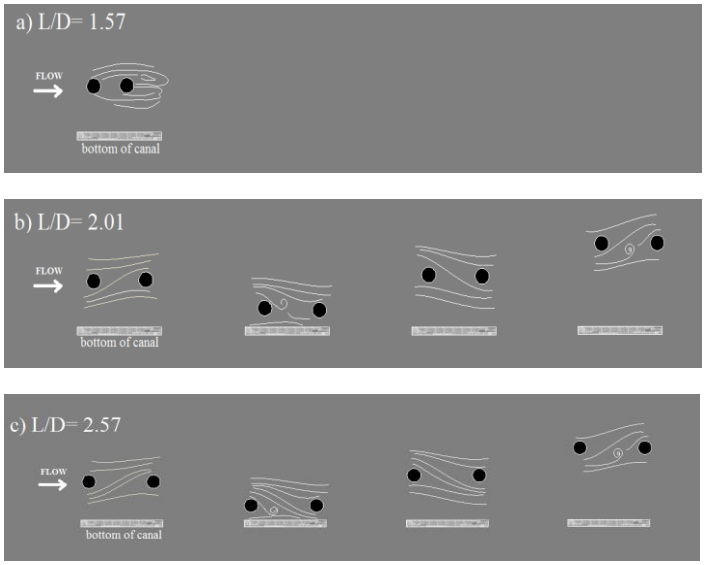

Figure 8. Schematic flow pattern around two tandem cylinders for spacing **a)** *L/D* = 1.57 **b)** *L/D* = 2.01 **c)** *L/D* = 2.57

When both cylinders moving toward the bottom of the channel, flow interaction would be similar to Figure 8-b and c. The flow sheds from the bottom of the upstream cylinder and takes the downstream cylinder down. The large transverse component of fluid-dynamic force is produced tending to push the downstream cylinder back towards the tandem arrangement. During moving both cylinders down, a vortex sheds from upstream cylinders and goes through both cylinders. This vortex changes the direction of flow pattern. This pattern continues until both cylinders reach the bottom wall limitation, the upstream cylinder starts changing the direction and moving up. At this time, a vortex sheds from the bottom of the upstream cylinders and moves between two tandem cylinders. So, the flow pattern completely changes for the second time. Again, the large transverse component of fluid-dynamic force is produced tending to push the downstream cylinder back towards the tandem arrangement. This flow pattern would continue as a cycle.

It can be concluded that since two cylinders act as a single body in L/D = 1.57, there is not any weakened galloping in harnessed power, but with increasing in L/D the flow pattern has totally changed and made the harnessed power decrease in velocity at some points. Figure 9 is an example of this decrease in harnessed power.

The black line indicates harnessed power for a single cylinder. A red line, blue line and green line present harnessed power for the upstream cylinder, downstream cylinder and synergy, respectively. As can be seen from Figure 9, there are five different branches including initial branch, upper branch and the lower branch, transition from VIV to galloping and galloping branches in this set-up. There is a big drop in the transition branch. But this drop is normal because of the transition from VIV to galloping. But it forms an extraordinary local drop in the galloping range for absolute velocity U = 1.15 m/s, reduced velocity U^* = 8.4 and Re = 103,000. This drop occurs in both downstream cylinder and upstream cylinder but especially deeper in the downstream cylinder. As can be seen from equation (10), harnessed power is firmly calculated with the square of the amplitude and oscillation frequency of the cylinders. Because of that reason, these results are investigated deeply in this paper. Figure 10- a and b and Figure 11- a and b show the amplitude and oscillation frequency of the cylinders for this set-up (m^* = 1.343, $\zeta_{harness}$ = 0.24 with K = 1,200 N/m spacing L/D = 2.57).

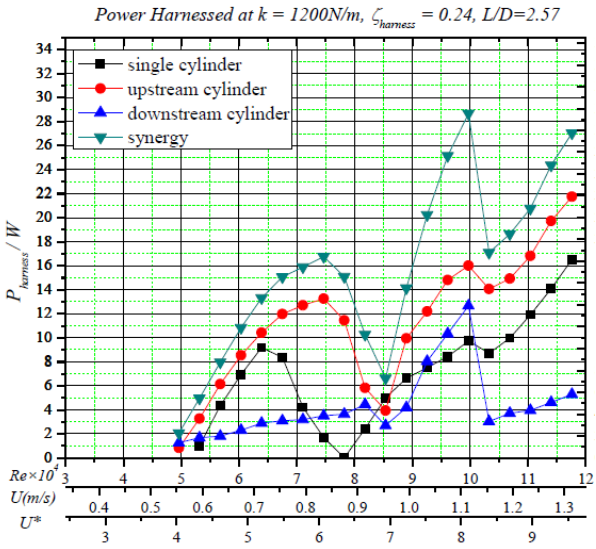

Figure 9. *Harnessed power curves for m* = 1.343 and $\zeta_{harness}$ = 0.24 with K = 1,200 N/m spacing L/D = 2.57 (Bernitsas, 2016b)*

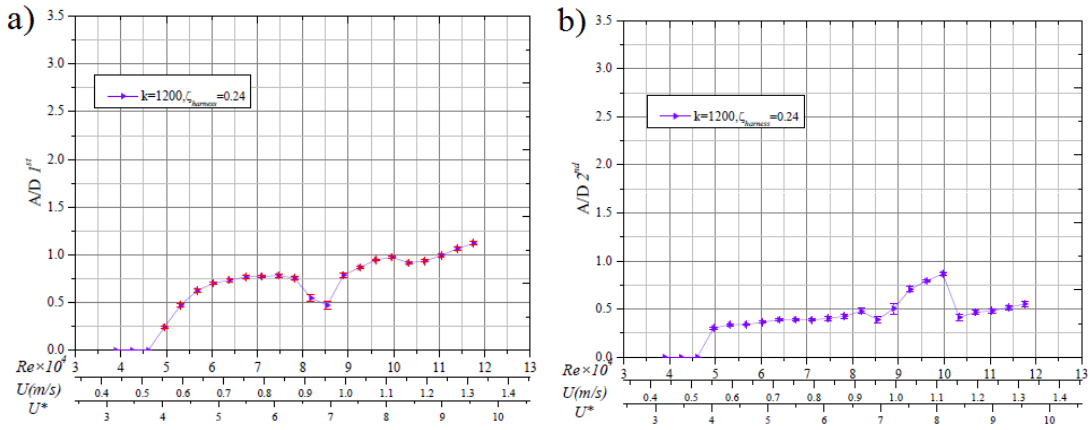

Figure 10. *Amplitude ratio (A/D) of the **a)** Upstream cylinder and **b)** Downstream cylinder for K = 1,200 N/m, $\zeta_{harness}$ = 0.24, L/D = 2.57*

Figure 10-a shows the amplitude ratio of the upstream cylinder for K = 1,200 N/m, $\zeta_{harness}$ = 0.24, L/D = 2.57. It can be easily seen that amplitude of the upstream cylinder decreases in the galloping range for absolute velocity U = 1.15 m/s. and also, there is a deep drop especially in the amplitude of the downstream cylinder at the same absolute velocity. There is a consistency between harnessed power and amplitude of the cylinders. Upstream cylinder affects downstream one negatively.

Figure 11 shows the amplitude ratio of the upstream and downstream cylinders for K = 1,200N/m, $\zeta_{harness}$ = 0.24, L/D = 2.57. In the drop region, there is no significant change in the frequency ratios. In the specific point which exists drop in the galloping range, galloping instability disappears.

Figure 12 displays the time history of the cylinders at the specific point before drop (Absolute velocity U = 1.10 m/s). The red line shows the amplitude of the upstream cylinder and the blue line indicates the amplitude of the downstream cylinder.

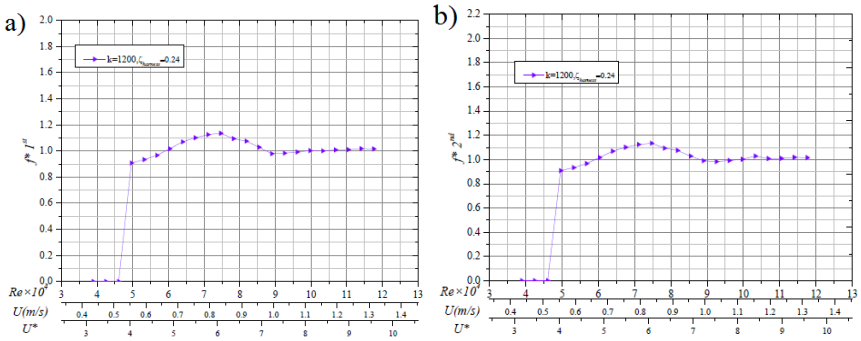

Figure 11. *Frequency ratio (f^*) of the* ***a)*** *Upstream cylinder and* ***b)*** *Downstream cylinder for K = 1,200 N/m, $\zeta_{harness}$ = 0.24, L/D = 2.57*

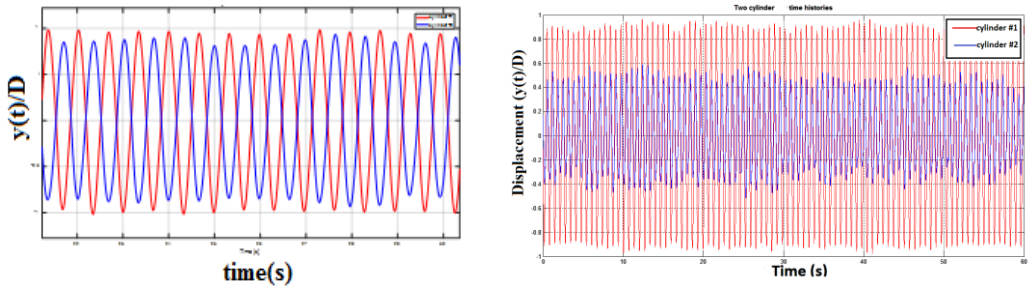

a. b.

Figure 12. Time history for two tandem cylinders before drop **a)** *U* = 1.10 m/s, *K* = 1,200 N/m, $\zeta_{harness}$ = 0.24 and *L/D* = 2.57 (for 60 seconds) **b)** *U* = 1.10 m/s, *K* = 1,200 N/m, $\zeta_{harness}$ = 0.24 and *L/D* = 2.57 (for 30 seconds)

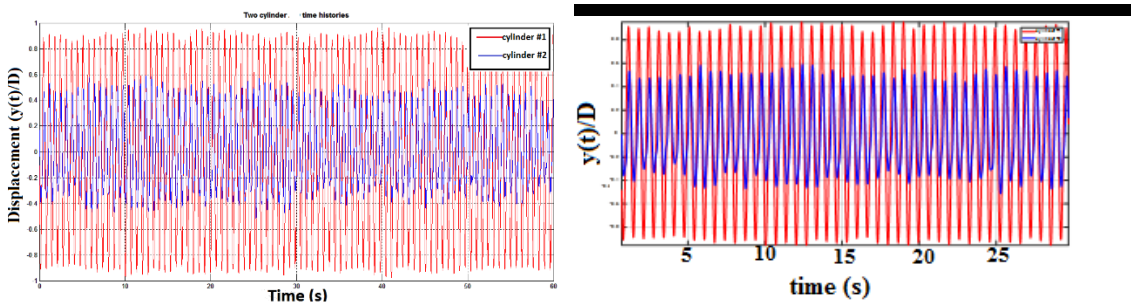

a. b.

Figure 13. Time history for two tandem cylinders at drop **a)** *U* = 1.15 m/s, *K* = 1,200 N/m, $\zeta_{harness}$ = 0.24 and *L/D* = 2.57 (for 60 seconds) **b)** *U* = 1.15 m/s, *K* = 1,200 N/m, $\zeta_{harness}$ = 0.24 and *L/D* = 2.57 (for 30 seconds)

Figure 13 indicates the time history of the cylinders at the specific drop point (Absolute velocity *U* = 1.15 m/s). The red line indicates the amplitude of the upstream cylinder and the blue line indicates the amplitude of the downstream cylinder.

As can be seen from Figure 12, the cylinders go up and down as out of phase before drop for *K* = 1,200 N/m, $\zeta_{harness}$ = 0.24, *L/D* = 2.57. They don't affect each other negatively. So that power harness and also amplitude ratios are increasing in a normal way. But on the other hand, the cylinders moves approximately in phase at the drop point (Figure 13) for the same set-up parameters. Upstream cylinder effects downstream cylinder negatively. There is a firm

interaction between cylinders. Galloping instability disappears at this point and harnessed power decreases sharply and amplitude as well.

5. CONCLUSION

Flow Induced Vibrations (FIVs) of two tandem, circular cylinder with end-springs are studied for 30,000<*Re* <120,000 with damping, stiffness and mass ratio as parameters in the LTFSW Channel of the Marine Renewable Energy Laboratory (MRELab). Typical local drops and jumps in harnessed power were observed in the velocity range of 0.9<*U*<1.2 m/s within the galloping region. The main goal of this paper is to explain the reason for the presence of these drops and jumps. For both upstream and downstream cylinders, time history graphs especially are investigated to define the reason of these drop/jumps. Before drop occurs, the cylinders go up and down as out of phase and they don't affect each other negatively. However, the cylinders moves approximately in phase at the drop point. Upstream cylinder affects downstream cylinder negatively. There is a firm interaction between cylinders. Galloping instability disappears at this point and harnessed power decreases sharply and amplitude as well. As a conclusion, there is a firm interaction between cylinders. Galloping instability disappears at this drops and harnessed power decreases sharply and amplitude as well.

ACKNOWLEDGEMENTS

The following support is gratefully acknowledged: Michael M.Bernitsas, Hai Sun, Kai Lan, Vida Atashi, Mert Turkol, Wenjun Ding and all MRELab personnel.

REFERENCES

1. Bernitsas, M. M., and Raghavan, K., (2007), "Reduction/Suppression of Vortex Induced Forces and Motion through Surface Roughness Control," *U.S. Provisional Patent Application* No. S2009/0114002 A1 (UofM#3757).

2. Bernitsas, M. M., Raghavan K., Ben-Simon Y., Garcia E.M.H., (2008), "VIVACE (Vortex Induced Vibration Aquatic Clen Energy): A New Concept in Generation of Clean and Renewable Energy from Fluid Flow" *ASME Paper* No. OMAE2008-041101-1. DOI: 10.1115/1.2957913

3. Bernitsas, M. M., and Raghavan, K., (2009), "Fluid Motion Energy Converter," *United States Patent and Trademark Office, Patent No*. 7,493,759 B2.

4. Bernitsas, M. M., and Raghavan, K., (2011), "Enhancement of Vortex Induced Forces and Motion Through Surface Roughness Control," *U.S. Patent Trademark Office, Patent No*. 8,042,232 B2.

5. Bernitsas, M. M., and Raghavan, K., (2014), "Reduction of Vortex Induced Forces & Motion Through Surface Roughness Control," *U.S. Patent and Trademark Office, Patent No*. 8,684,040 B2.

6. Bernitsas, M. M., (2016a), Harvesting Energy by Flow Included Motions (Chapter 47), *Handbook Ocean Engineering*, Springer.

7. Bernitsas, M. M., (2016b), Synergistic Flow-Induced Motion of Two Cylinders Harvesting Marine Hydrokinetic Energy, *METS* 2016.

8. Blevins R.D.: Flow-Induced Vibration (Krieger, Florida 1990).

9. Bokaian, A., and Geoola, F., (1984), Wake-Induced Galloping of Two Interfering Circular Cylinders, *Journal of Fluid Mechanics,* Vol.146, p.383–415. DOI:10.1017/S0022112084001920

10. Bokaian A., (1989), Galloping of a circular cylinder in the wake of another, *J. Sound Vib.* 128, 71–85. DOI:10.1016/0022-460X(89)90681-0

11. Chang C.C. (2010), Passive turbulence control for VIV enhancement for hydrokinetic energy harnessing using vortex Induced vibrations, *Ph.D. thesis*. Ann Arbor, MI: The University of Michigan.

12. Chang, C. C., and Bernitsas, M. M., (2011), "Hydrokinetic Energy Harnessing Using the VIVACE Converter With Passive Turbulence Control," ASME Paper No. *OMAE2011*-50290. DOI:10.1115/OMAE2011-50290

13. Ding L, Bernitsas M.M., Kim E.S., (2013), 2-D URANS vs. experiments of flow induced motions of two circular cylinders in tandem with passive turbulence control for 30,000 < Re < 105,000. *Ocean Engineering* 2013;72:429–40. DOI:10.1016/j.oceaneng.2013.06.005

14. Ding L, Zhang L, Kim E.S, Bernitsas M.M., (2015), URANS vs. experiments of flow induced motions of multiple circular cylinders with passive turbulence control. *J Fluid Struct*;54:612–628. DOI:10.1016/j.jfluidstructs.2015.01.003

15. Ishigai S., Nishikawa E., Nishimura E. and Cho K., (1972), Experimental study of structure of gas flow in tube banks axes normal to flow: Part1, Karman Vortex flow from two tubes at various spacings, *Bulletin of the Japan Society of Mechanical Engineering*, 15(86), 949-956. DOI: 10.1299/jsme1958.15.949

16. Kim ES, Bernitsas MM, Kumar AR., (2013), Multi-cylinder flow induced motions: enhancement by passive turbulence control at 28,000 < Re < 120,000. *J Offshore Mech Arct Eng* 2013;135:021802. DOI: 10.1115/1.4007052

17. Kim, E. S and . Bernitsas, M. M. (2016), Performance prediction of horizontal hydrokinetic energy converter using multiple-cylinder synergy in flow induced motion. *Applied Energy*, 170 (2016) 92–100. DOI: 10.1016/j.apenergy.2016.02.116

18. Kinaci O.K., Lakka S., Sun H., Fassezke E., Bernitsas M.M. (2016), Computational and Experimental Assessment of Turbulence Stimulation on Flow Induced Motion of a Circular Cylinder. ASME. J. Offshore Mech. Arct. Eng. 2016;138(4):041802-041802-9. DOI:10.1115/1.4033637.

19. Lee J.H, Xiros N, Bernitsas M.M., (2011), Virtual damper-spring system for VIV experiments and hydrokinetic energy conversion. *Ocean Engineering*;38:732–47. DOI:10.1016/j.oceaneng.2010.12.014

20. Lee J.H, Bernitsas M.M., (2011) High-damping, high-Reynolds VIV tests for energy harnessing using the VIVACE converter, *Ocean Engineering*;38: 1697–712. DOI:10.1016/j.oceaneng.2011.06.007

21. NREL: Renewable electricity futures study, Vol. 2, Renewable electricity generation and storage technologies, http://nrel.gov/analysis/re-futures/(2012).

22. Park H., (2012), Mapping of Passive Turbulence Control to Flow Induced Motions of Circular Cylinders,*Ph.D. dissertation*, The University of Michigan.

23. Park H, Bernitsas MM, Kumar RA., (2012), Selective roughness in the boundary layer to suppress flow-induced motions of a circular cylinder at 30,000 < Re < 120,000. *J Offshore Mech Arct Eng*;134:041801. DOI: 10.1115/1.4006235

24. Park H, Bernitsas MM, Chang CC., (2013a), Robustness of the map of passive turbulence control to flow-induced motions for a circular cylinder at 30,000 < Re < 120,000. In: Proceedings of the 31st *OMAE* 2013 conf., Paper #10123, Nantes, France; June 9–14, 2013.

25. Park H., Bernitsas M.M., Kumar R.A., (2013b), Enhancement of flow-induced motion of rigid circular cylinder on springs by localized surface roughness at $3.0x10^4$ <Re<$1.2x\ 10^5$. *Ocean Engineering*; 72:403–15. DOI:10.1016/j.oceaneng.2013.06.026

26. Park H, Bernitsas MM, Kim ES., (2013c), Selective surface roughness to suppress flow induced motions of two circular cylinders at 30,000 < Re < 120,000, *OMAE2013* 10125, June 9-14, 2013, Nantes, France.

27. Raghavan, K.,(2007), Energy Extraction From a Steady Flow Using Vortex Induced Vibration, *Ph.D. thesis*, The University of Michigan, Ann Arbor, MI.

28. Richardson A.S., Martucelli J.R., Price W.S., (1965) Research study on galloping of electric power transmission lines, *Proc. 1st Int. Conf. Wind Eff. Build. Struct*.'65: pp. 612–686.

29. Sun, Q., Alam, Md. M., Zhou, Y., (2015a), Fluid-Structure Coupling between Two Tandem Elastic Cylinders, *Procedia Engineering*, Vol. 126, p.564-568. DOI:10.1016/j.proeng.2015.11.306

30. Sun H, Kim E.S, Bernitsas P.M., Bernitsas M.M., (2015b), Virtual spring-damping system for flow-induced motion experiments. *J Offshore Mech Arct Eng*; 137:061801. DOI:10.1115/1.4031327

31. Sun, H., Ma, Ch., Kim, E. S., Nowakowski, G., Mauer, E., Bernitsas, M. M., (2017), Hydrokinetic energy conversion by two rough tandem-cylinders in flow induced motions: Effect of spacing and stiffness, *Renewable Energy*, 107,61-80. DOI:10.1016/j.renene.2017.01.043

32. Unal M.F, Rockwell D., (1988), On vortex formation from a cylinder, Part 1: The initial instability, *J. Fluid Mech*. 190, 491–512. DOI:10.1017/S0022112088001429

33. Wu W, Bernitsas MM, Maki K., (2011), RANS simulation vs. experiments of flow induced motion of circular cylinder with passive turbulence control at 35,000 < Re < 130,000. In: *ASME* 2011 30th International conference on ocean, offshore and arctic engineering, Rotterdam, The Netherlands. DOI: 10.1115/1.4027895

34. Wu W., (2011), Two-dimensional RANS simulation of flow-induced motion of circular cylinder with passive turbulence control. *Ph.D. thesis*, University of Michigan.

35. Xu G., Zhou Y., (2004), Strouhal numbers in the wake of two inline cylinders, *Experiments in Fluids* 37, 248-256. DOI:10.1007/s00348-004-0808-0

36. Zhou Y., Yiu M.W., (2006), Flow structure, momentum and heat transport in a two tandem cylinder wake. *Journal of Fluid Mechanics* 548, 17-48. DOI:10.1017/S002211200500738X

37. Zdravkovich, M.M., (1987), The effects of interference between circular cylinders in cross-flow, *Journal of Fluids and structures*, 239-261. DOI:10.1016/S0889-9746(87)90355-0

38. Zdravkovich M.M.: Flow Around Circular Cylinders, Vol. 1 (Oxford Univ. Press, Oxford 1997)

39. Zdravkovich M.M.: Flow Around Circular Cylinders, Vol. 2 (Oxford Univ. Press, Oxford 2002)

40. Vikestad K., Vandiver J.K., and Larsen C.M., (2000), Added Mass and Oscillation Frequency for a Circular Cylinder Subjected to Vortex-Induced Vibrations and External Disturbance, *J. Fluids Struct*., 14(7), pp. 1071–1088. DOI:10.1006/j#s.2000.0308